Space Weather

RESEARCH ARTICLE
10.1029/2023SW003596

Measurements of Cosmic Rays by a Mini-Neutron Monitor at Neumayer III From 2014 to 2017

M. Walter[1], C. Gnebner[2], B. Heber[2], K. Herbst[2], H. Krüger[3], H. G. Krüger[3], P. Kühl[2], H. P. Prokoph[1], and R. D. Strauss[3]

[1]Deutsches Elektronen-Synchrotron DESY, Zeuthen, Germany, [2]Institut für Experimentelle und Angewandte Physik, Christian-Albrechts Universität zu Kiel, Kiel, Germany, [3]Center for Space Research, North-West University, Potchefstroom, South Africa

Key Points:

- Measurements of Galactic Cosmic Rays by a mini-neutron monitor (MNM) at the German Antarctic Research Station from 2014 to 2017 are presented
- The measurements were successfully corrected for pressure and normalized to the weighted mean of the SANAE and TERA Neutron Monitor
- We show that Forbush Decreases with amplitudes above 3% in Magnitude identified by the IZMIRAN database can be identified with the MNM too

Correspondence to:
B. Heber,
heber@physik.uni-kiel.de

Citation:
Walter, M., Gnebner, C., Heber, B., Herbst, K., Krüger, H., Krüger, H. G., et al. (2024). Measurements of cosmic rays by a mini-neutron monitor at Neumayer III from 2014 to 2017. *Space Weather*, *22*, e2023SW003596. https://doi.org/10.1029/2023SW003596

Received 12 JUN 2023
Accepted 17 APR 2024

Author Contributions:
Conceptualization: B. Heber, H. Krüger
Data curation: M. Walter, B. Heber
Formal analysis: M. Walter, B. Heber
Investigation: M. Walter
Project administration: C. Gnebner
Resources: H. G. Krüger, R. D. Strauss
Software: M. Walter, B. Heber, H. G. Krüger, R. D. Strauss
Supervision: H. Krüger
Validation: H. P. Prokoph
Visualization: M. Walter, B. Heber
Writing – original draft: M. Walter, B. Heber
Writing – review & editing: H. Krüger, H. G. Krüger, P. Kühl, R. D. Strauss

Abstract A mini-neutron monitor (MNM) was installed at the German Antarctic Neumayer III station, measuring the variation of galactic cosmic rays and searching for Forbush Decreases (FDs) caused by solar activities. Running continuously from 2014 until the end of 2017, the long-term stability of the detector could be investigated. After correcting the air pressure and normalization to the 27 days running mean averages of the SANAE and TERA Neutron Monitors (NMs), the daily running mean count rates are compared with the SANAE and TERA NMs also installed in Antarctica. For most of the 14 FDs with magnitudes greater than 3, taken from the list compiled by the IZMIRAN group (http://spaceweather.izmiran.ru/eng/dbs.html), the three detectors show consistent particle flux variation, although the average rate of the MNM is more than a hundred times smaller. The light and low-cost MNM is an ideal alternative to heavy and old NMs, especially at high altitudes and remote environments.

Plain Language Summary A mini-neutron monitor (MNM) was installed at the German Antarctic Neumayer III station from 2014 till the end of 2017, measuring the variation of galactic cosmic rays and investigating its sensitivity by searching for Forbush decreases (FDs). The data were successfully corrected for pressure and normalized to the long-term trend utilizing 27-day running mean averages of the weighted mean of SANAE and TERA NMs. A comparison with the SANAE and Terre Adelie NMs on the basis of daily running mean averages reveals a difference of about 1% for each combination. Utilizing the IZMIRAN FD catalog, we showed that the sensitivity of the MNM is large enough to investigate FDs with amplitudes above 3%, making the MNM a useful instrument for space weather investigations.

1. Introduction

Ground-based measurements of Galactic Cosmic Rays (GCRs) have been performed since their discovery by Viktor Hess in 1912. Since the 1950s, the efficient detection of neutrons with Neutron Monitors (NMs) has allowed detailed investigations of effects concerning the hadronic components of the Solar Energetic Particles (SEPs) and of GCRs (Shea & Smart, 2000; Simpson, 2000). Because NMs are integral counters with a threshold energy defined by the minimum of the magnetic cut-off energy and the shielding by the atmosphere, neither the energy spectra nor anisotropies of GCRs and SEPs during a Ground Level Enhancement (GLE) can be determined by a single NM. Therefore, several of the NMs have been installed worldwide and utilized to characterize the particle distribution (see e.g., Bieber et al., 2004; Matthiä et al., 2009; Mishev et al., 2018 and references therein).

To calibrate the worldwide distributed NMs against each other, the North-West University in Potchefstroom, South Africa, proposed the development of a calibration NM (Moraal et al., 2000). A portable detector, hereafter called a Mini-Neutron Monitor (MNM), has been realized (see also Krüger et al., 2008; Moraal et al., 2003; Strauss et al., 2020 and references therein). Measurements with NMs are influenced by the variable Earth's magnetic field and the atmospheric conditions close to its position. This requires for the Mini Neutron Monitors (MNMs) a detailed knowledge of the instrument sensitivity with geomagnetic latitude (rigidity), atmospheric pressure as well as temporal variations of the environment.

In this paper, data will be analyzed taken from 2014 to 2017 with an MNM installed at the German Antarctic Neumayer III research station of the Alfred-Wegener-Institute (https://www.awi.de/en/expedition/stations/neumayer-station-iii.html). As can be seen from Figure 1, the considered time was during solar cycle 24 starting in

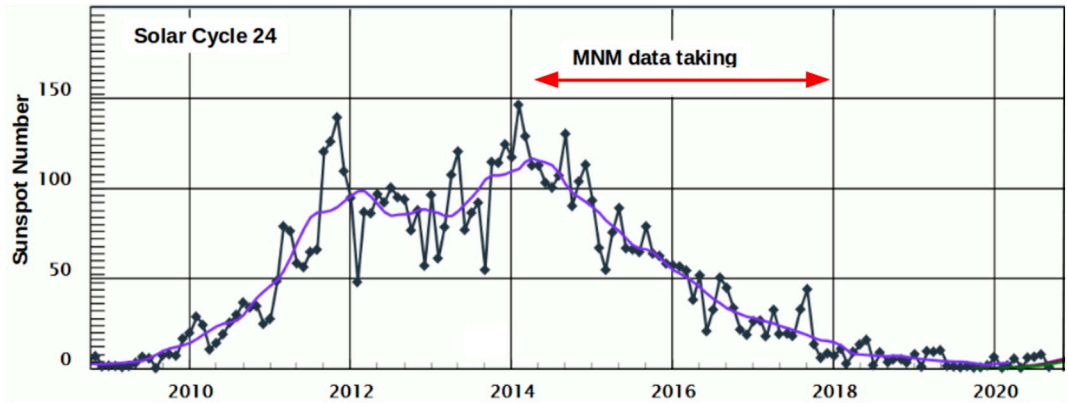

Figure 1. The monthly sunspot number for solar cycle 24 with the data-taking period of the mini-neutron monitor. The figure was taken from the Space Weather Prediction website (https://www.swpc.noaa.gov/products/solar-cycle-progression).

March 2014, and ending on 31 December 2017. The sunspot number reached its maximum in 2014 with an average number of 113 spots per month and went down continuously to 23 spots per month in 2017.

The focus of this paper is on the investigation of the long-term stability of an MNM (Section 1) and its sensitivity by comparing the measured particle rates with those of NMs also installed at sea level (Section 2). Furthermore, we will look in Section 3 for physical effects caused by the solar wind as the FDs. Within our data-taking time (2014–2017), only one GLE was detected. The GLE-72 was identified by several NMs, including the TERA reference detector, and also the two MNMs DOMB and DOMC installed at an altitude of 3,200 m in Antarctica. The count rate of the MNM at sea level and DOMC is about 0.9 count/sec and 18 counts/sec, respectively. Mishev et al. (2018) investigated the event based on 15-Minute averages and found for DOMC an increase of 9% with a statistical precision of less than 1%. The count rate statistics of our MNM is about 3.5%. Thus, we should have observed an increase if the flux variation had been as high as 9%. However, Mishev et al. (2018) showed a strong anisotropy of the event with an increase of about 4% at the South Pole NM. Thus, the expected increase is less than that at DOMC, and therefore, the statistical accuracy is too low to see a significant rate increase based on 15-min averages. The last section summarizes the results and gives some conclusions for promising future installations of MNMs. The rigidity dependence at sea level is determined experimentally by utilizing so-called latitude scans with a MNM installed on the German research vessel Polarstern (https://www.awi.de/en/expedition/research-vessel-and-cutter/polarstern.html) and will be published in a separate paper.

2. Investigation of the Long-Term Stability of the MNM

At the end of 2012, a MNM was installed at the Neumayer III station, which is located on the Ekström-shelf-ice in the Atka-bay of Antarctica at about 17 m above sea level. For the station position 70°40 S and 8°16 W, a cut-off rigidity of R_C 0.6 to R_C 0.7 GV for 1 January 2024 and an IOPT of 2 has been calculated utilizing Planetocosmics (Desorgher et al., 2009) and Oulu—Open-source geomagneToSphere prOpagation tool (OTSO) (Larsen et al., 2023) with the International Reference Geomagnetic Field (IGRF) and the (Tsyganenko, 1989) model for the inner and outer Earth magnetosphere, respectively.

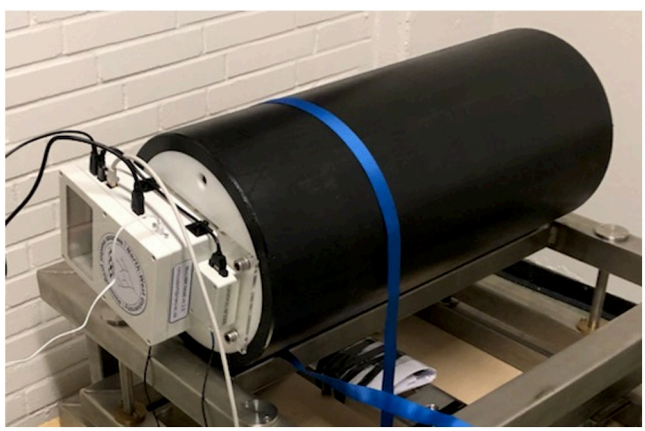

Figure 2. Picture of the mini-neutron monitor (MNM). The gray electronics box in front of the tube is not the box used for the MNM at the Neumayer Station, but the newer one, working with other MNMs since 2019.

Figure 2 shows the cylindrical MNM with a length of 800 mm, 400 mm diameter, and a weight of 250 kg. The gray box on the left contains the electronics. Details of the mechanical design, the electronics, and functionality are given in Strauss et al. (2020). Therein the new electronic head is characterized that was introduced in 2017 (Krüger et al., 2017). However, the Neumayer MNM used the older version of the electronics as described in Krüger et al. (2013, 2015) and Heber et al. (2015). In December 2013, the LND20366 counter was replaced by the newer LND2043 counter (for details,

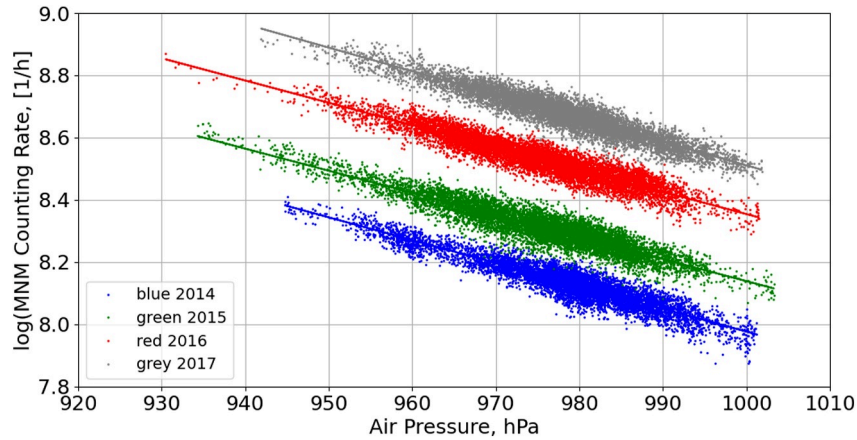

Figure 3. Dependence of the natural logarithm of the raw mini-neutron monitor particle rates on the air pressure for the years 2014–2017.

see Krüger et al., 2013). Since the data from 2012 to 2013 are not compatible, the analysis presented in the following uses only data recorded with the new tube from March 2014 until the end of 2017.

2.1. Air Pressure Dependence of Particle Rates

The air pressure correction of the MNM particle rates was performed for the years 2014–2017 separately using the pressure measured inside by the MNM detector. The air pressure measured outside the Neumayer Station can be influenced by the wind speed. Figure 3 presents the natural logarithm of the count rate in dependence on the air pressure for the 4 years, together with the straight line of the linear regression. The fitted mean values and standard deviations of the air pressure and the fitted slopes of the MNM rate dependence on the air pressure are summarized in Table 1. As can be seen, the spread of the pressure mean values is rather small, whereas the values of the barometric coefficients β show larger deviations. Therefore, the pressure correction of the MNM rate $Rate_{measured}$ was performed with the mean values for pressure of 977 hPa and slope β 0.00708 (last column in Table 1) computed from the yearly values using the formulae:

$$Rate_{p\ corrected} \quad Rate_{measured} \cdot \exp(\ \beta \cdot (p \quad p_{mean})).$$

The air pressure corrected MNM counting and the raw data are presented in Figure 4. As discussed in Strauss et al. (2020), the count rates of a NM are affected by temperature variations and variations of the High Voltage (HV) (see also Krüger et al., 2008, and references therein). The MNM on Neumayer III was installed in a room where the temperature varies with the outside temperature. The maximum room temperature was about 28°C in Antarctic summer and about 12°C in winter. The MNM worked in the years 2014–2017 with the older electronic box, where the HV increased with rising room temperature, which led to an increase in the count rate. In Appendix A, the influence on the pressure-corrected count rate is discussed, but the effect is too small to modify the rate distribution. Therefore, it was decided to compare the MNM count rates for the years 2014–2017 with the count rates of other NMs.

Table 1
Fit Values for the Different Years 2014–2017

Fit results	2014	2015	2016	2017	Mean value (2014–2017)
Mean Value p, hPa	978.8	975.4	974.9	978.2	976.8
Standard Deviation	9.7	10.0	9.6	9.3	
Slope β, 1/hPa	0.00734	0.00695	0.00687	0.00714	0.00708
Error	0.00003	0.00003	0.00003	0.00003	

Note. Rows 2 and 3: Mean value and standard deviation of the air pressure distributions. Rows 4 and 5: The barometric coefficient and error of the fits to the yearly distributions: log(MNM-Rate vs. Air Pressure) shown in Figure 3.

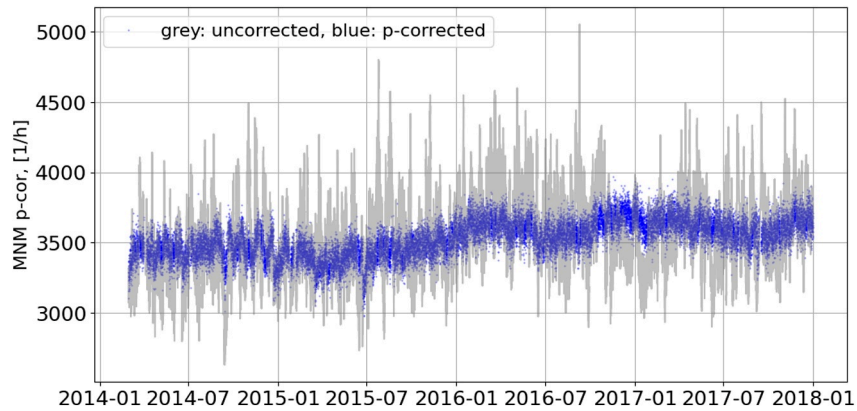

Figure 4. Uncorrected mini-neutron monitor particle rate (gray) and pressure-corrected count rate (blue) for the years 2014–2017.

2.2. Pressure Corrected MNM Count Rates

The results of the air pressure corrections are shown in Figure A3. The variation of the uncorrected count rate (gray) is reduced by more than a factor of two. The air pressure corrected count rate (blue) were almost flat in 2014. For the first half of 2015, stronger fluctuations were observed, followed by an increase in the second half. As will be seen later, such an increase is also observed by other NMs. Although corrected by utilizing the long-term variation, as shown in the following section, the temperature dependence of the HV and its influence on the count rate is clearly visible for 2016 and 2017 with lower rates in wintertime.

3. Comparison of Particle Rates With the TERA and SANAE NMs

The comparison of the MNM count rate will be performed with two NMs also installed in Antarctica: The TERA NM on the French Dumont d'Urville research station at sea level, and the SANAE NM on the South African SANAE IV base at a medium altitude with a distance of about 300 km from the MNM. Table 2 presents the geographic position, the altitude above sea level, the cut-off rigidity R_c, and the mean count rates for the three detectors.

The TERA and SANAE NMs were chosen for comparison since the NMs at sea level and 856 m altitude are shielded by an atmosphere of more than 950 hPa corresponding to a rigidity of about 1 GV (Poluianov et al., 2017). Thus, the atmospheric shielding dominates the geomagnetic one for cut-off rigidities below 1 GV (see, for example, Mishev et al. (2018) and references therein). To compare the count rate distributions of the three detectors, the average rates have been calculated for the four years 2014–2017 (see Table 2) and used to normalize the corresponding count rates per hour.

The statistical fluctuations could be reduced by calculating the 1-day running mean, especially for the MNM count rate (see Table 3), which is reduced from about 2.2% to about 0.6% that is in the range of the 1 SD values for SANAE and TERA.

In the upper diagram of Figure 5, the normalized 1-day running mean count rates are shown for the MNM, the TERA, and the SANAE detector. The agreement is rather good for the years 2014 and 2015, but strong deviations are visible in the following two years. While the MNM count rate drops mid 2016 and increases late 2016 the count rates for TERA and SANAE are increasing continuously. A similar feature can be observed in 2017. The

Table 2
The Characteristic Data of the Two Neutron Monitors SANAE, TERA and the Mini-Neutron Monitor Used in the Analysis

Neutron monitor	Latitude	Longitude	Rigidity [GV]	Altitude [masl]	Mean rate 2014–2017 [Hz]
MNM	70°40 S	8°16 W	0.1	17	0.98
SANAE	71.67 S	2.85 W	0.73	856	164.6
TERA	66.65 S	140 E	0.01	32	115.2

Table 3
The Mean Values and Statistical Uncertainties (1 Standard Deviation) of the Counting Rates per Hour for the Mini-Neutron Monitor, SANAE, and TERA for Four Periods in 2014–2017

	NM	2014		2015		2016		2017	
Normalized rate per h	MNM	0.983	0.019	0.963	0.022	1.025	0.022	1.035	0.021
Mean 1 SD	SANAE	0.964	0.007	0.977	0.009	1.011	0.008	1.040	0.007
	TERA	0.967	0.005	0.969	0.007	1.017	0.008	1.048	0.007
Normalized rate per h	MNM	0.983	0.006	0.963	0.008	1.025	0.007	1.035	0.005
Mean 1 SD	SANAE	0.964	0.005	0.978	0.007	1.110	0.006	1.040	0.005
(1-day running Mean)	TERA	0.967	0.004	0.969	0.006	1.017	0.007	1.048	0.006

Note. The last three rows show the improvements using the 1-day running mean.

discrepancy is even more pronounced and visible in the distributions of the lower panel, which shows the count rates of the three monitors for the 27-day running mean. Note, that due to longer data gaps two periods have been removed from the analysis as indicated by the two boxes. This effect can not be explained by the observed

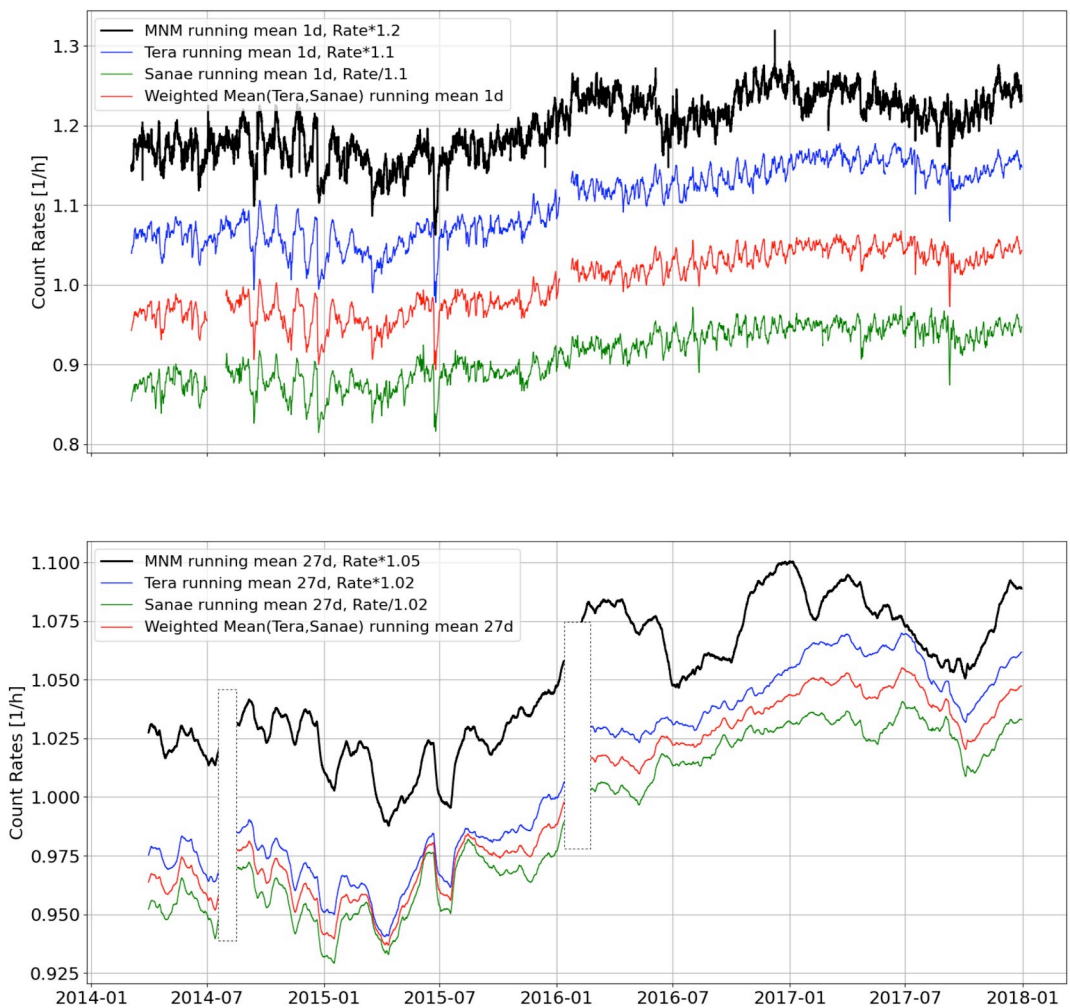

Figure 5. The upper panel displays the normalized and daily averaged count rates of the mini-neutron monitor (black curve), the TERA (blue), and the SANAE (green). The red curve presents the WM(TERA, SANAE) rates. In the lower panel, the same counting rates are shown with a running mean over 27 days. Note, that two periods for which SANAE or TERA had long data gaps have been indicated by the boxes.

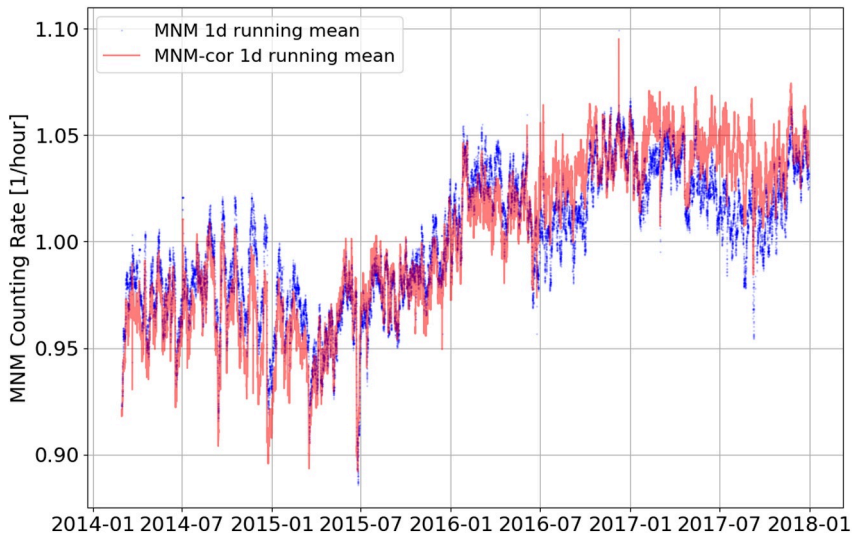

Figure 6. The 1-day running mean count rate distributions of the air pressure corrected mini-neutron monitor (blue) and in red the MNM-cor WM(TERA, SANAE) corrected distribution.

temperature/HV effect discussed in Appendix A. Since we could not monitor and control possible effects inside or outside the Neumayer Station during the four years, it is not excluded that unknown effects could have influenced the MNM count rate, especially in 2016 and 2017. Note, as discussed below we find some small deviations in 2014 too.

3.1. Correction of the MNM Measurements by Utilizing a Reference Monitor

Therefore, an adjustment of MNM distribution to those of TERA and SANAE was performed. The weighted mean of the TERA and SANAE count rates (in the following: WM(TERA, SANAE) was calculated for the 27-day running mean. The resulting distribution, shown as a red curve in the lower panel of Figure 5, was used for correcting the MNM count rate. The WM(TERA, SANAE) 1-day running mean distributions in the upper panel show that all fine structures of the distribution remain. This gives the confidence that a correction using the WM (TERA, SANAE) 27-day running mean distribution influences only the general shape of the MNM count rate distribution.

The correction effect can be seen in Figure 6 where the 1-day running mean MNM count rate is displayed together with the MNM WM(TERA, SANAE) correction, hereinafter referred to as MNM-cor. There are small deviations in 2014 and stronger ones in 2016 and 2017.

An additional possibility to prove the quality of the correction method gives the ratio distributions of the normalized 1-day running mean count rates presented in Figure 7. The r(MNM-cor)/r(SANAE) and r(MNM-cor)/r(TERA) ratios in the upper and middle panels show less pronounced structures than the r(TERA)/r(SANAE) distribution in the lower panel.

3.2. Discussion of the MNM Solar Cycle Observations

The corrected MNM count rates increased from April 2015 until the beginning of 2016 in correspondence with the 11-year solar cycle. The 24th cycle (2009–2019) had its sunspot maximum in 2014 (see Figure 1). Higher solar activity in 2014 and 2015 was connected with a higher solar wind velocity and a stronger heliospheric magnetic field near Earth. Both modulate the cosmic particle rates measured on Earth, leading to a rate reduction, as will be discussed later in the following section about FDs. In Figure 8, the monthly values of the force field modulation parameter ϕ, reconstructed from ground-based cosmic ray data (see Usoskin et al. (2011) and references therein) are presented by the "mirrored" ϕ values:

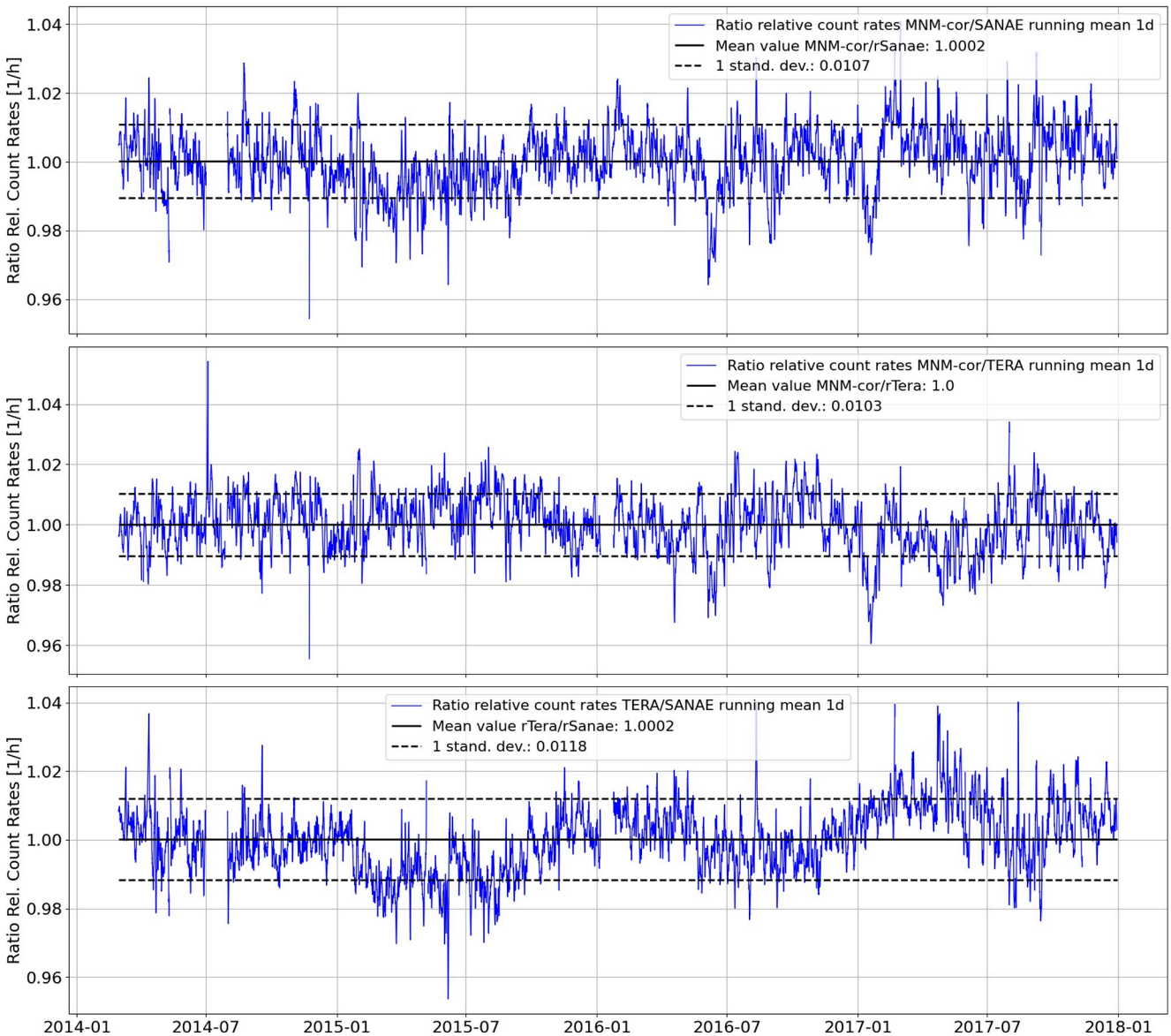

Figure 7. Upper distribution: Ratios of normalized count rates r(MNM-cor)/r(SANAE). Middle: r(MNM-cor)/r(TERA). Lower distribution: r(TERA)/r(SANAE). The solid line is the mean value, while the dashed lines indicate the one standard deviation.

$\phi_{mirrored}$ ϕ_{mean} ϕ with the mean value of ϕ_{mean} 528.94 MV. The comparison of the 27-day running means MNM-cor count rate with the"mirrored" ϕ distribution shows a rather good agreement. In addition, the WM (TERA, SANAE) distribution is displayed, which must agree naturally with MNM-cor.

4. Forbush Decreases

Forbush (1937) and Hess and Demmelmair (1937) were the first to observe short-term flux decreases of GCRs using ionization chambers. Several studies on FDs have been performed since then utilizing NMs and space instrumentation (see for example Blanco et al. (2013); Melkumyan et al. (2019); Dumbović et al. (2012) and references therein). A comprehensive review on this topic has been given by Cane (2000) and by Richardson and Cane (2011). Typical amplitudes for FDs vary between less than a percent and a few 10 percent (Wang et al., 2023). Because FDs can be attributed to interplanetary structures, they are ideally suited to investigate the sensitivity of the Neumayer MNM. Due to its high count rate variability, as discussed above, the measurements themselves are not suitable for FD detection. However, if a FD has been detected by

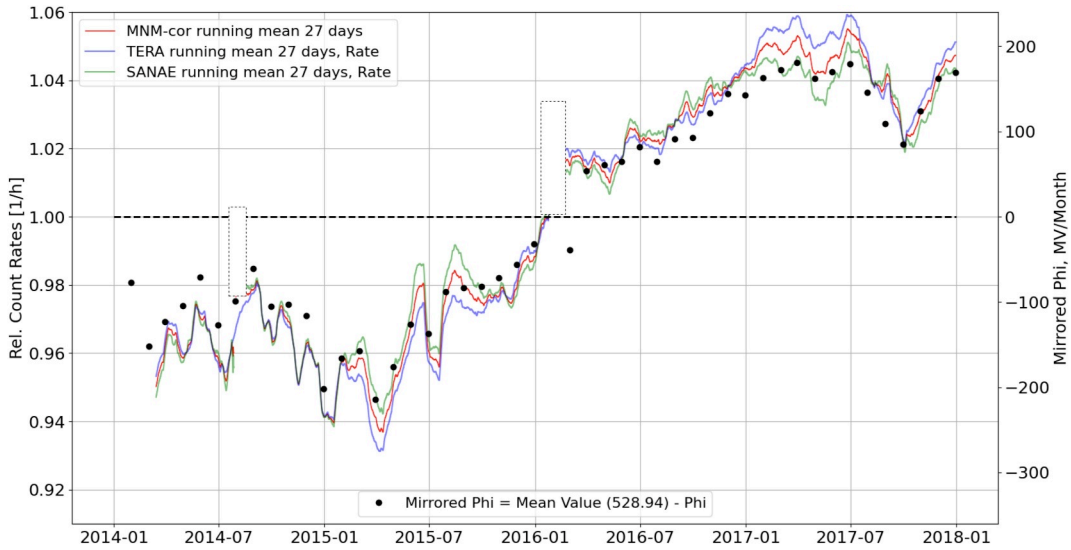

Figure 8. The 27-day running mean distributions of MNM-cor (red curve), TERA (blue curve) and SANAE (green curve) in comparison with the "mirrored" force field modulation parameter ϕ (black points). Note, that two periods for which SANAE or TERA had long data gaps have been indicated by the boxes.

other means, the count rates could be compared to the one of other NMs. In this study, we use the SANAE and TERA NMs.

As shown above, the hourly averaged count rates of the MNM have a statistical uncertainty σ 2%. If a measured decrease should be significant, the amplitude $\frac{\Delta C}{C}$ should be larger than 3σ corresponding to $\frac{\Delta C}{C} \geq 6\%$. Thus, the number of FDs to investigate would shrink to 2 according to a database compiled by the IZMIRAN group (Belov, 2009). The statistical fluctuations could be reduced by calculating the 24-hr running mean averages. Table 3 presents the particle rate mean values and the standard deviation values for four periods where the rates are approximately constant excluding FDs or systematical rate variations. The statistical uncertainties of the MNM are reduced from about 2.2% to about 0.6%. Running mean averaging acts as a low pass filter, suppressing the high-frequency signals (Eckner, 2015). Because each value depends on the ones measured before and after the specific hour, the uncertainty is larger than the statistical one. Figure 7 shows the ratio of the MNM to the other two NM with typical fluctuation on the one percent level:

FDs with amplitudes larger than 3.0% from the IZMIRAN database (http://spaceweather.izmiran.ru/eng/dbs.html) are investigated to estimate the sensitivity of the MNM. This list provides, among others, the MagnM, the maximum count rate decrease, that is determined as the magnitude of the FD for cosmic rays with a rigidity of about 10 GV taking into account magnetospheric effects (for details see Belov (2009) and references therein). Table 4 summarizes the number of FDs for different ranges of the parameter MagnM from March 2014 to the end of 2017, corresponding to the measurement period of the Neumayer MNM. In total, 553 FDs were reported during the Neumayer MNM period from which 14 events had MagnM >3. In 2014, solar cycle 24 reached its maximum with 124 FDs from March to December. In 2014/2015 and 2016/2017, the number of FDs with MagnM >3.0 was twelve and two, respectively. This shows the solar cycle dependence of the occurrence of FDs (Lingri et al., 2016). In the following, these 14 FDs will be presented and discussed in more detail.

Table 4
Total Number of Forbush Decrease (FD) per Year and Number of FD for Different Magnitude Ranges

Year	Total no.	>3–4	>4–5	>5–6	>6–7	>7–8	>8–9	>9–10
≥03/2014	124	4	0	2	0	0	0	0
2015	149	3	0	2	0	0	0	1
2016	151	0	0	0	0	0	0	0
2017	129	0	0	1	0	1	0	0

Note. The data were taken from the IZMIRAN FD database.

In what follows, the corrected normalized count rate MNM-cor is compared with those of the SANAE and TERA NMs. The normalization is performed so that the average count rate over the full measurement period becomes one. For all the following figures, the rates are given as 24-hr (1-day) running mean values. Figures 9 and 10 show the count rate time profile for the years 2014, 2015 and 2016, 2017, respectively. To distinguish between the different NMs,

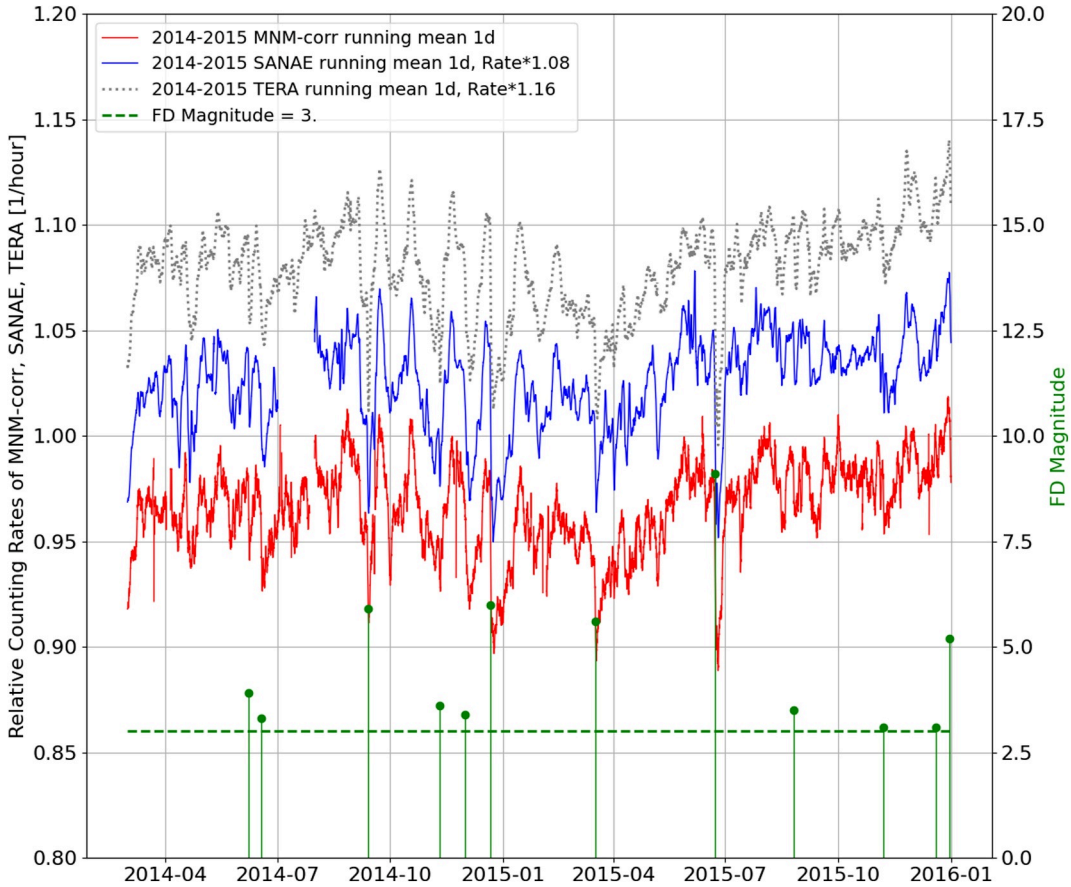

Figure 9. The 1-day running mean particle rates of the mini-neutron monitor, SANAE, and TERA Neutron Monitor for the years 2014 and 2015. The onset times of the Forbush Decreases with magnitudes MagnM >3 are indicated by green lines. The height of these vertical lines characterizes the magnitudes.

the normalized count rate of TERA and SANAE have been multiplied by 1.16 and 1.08, respectively. The 14 FDs with a magnitude MagnM >3 are marked by vertical green bars. From both figures, it is evident that count rate profiles show rather strong fluctuations that can either be caused by real FDs or by magnetospheric, atmospheric, instrumental, and environmental effects.

For a more detailed investigation of the 14 events, periods of about four weeks are chosen and summarized in Figures 11 and B1–B10. These figures display the daily running mean averaged count rates for the MNM (red curve), the SANAE (blue curve), and the TERA (gray curve) detectors based on hourly averages. Vertical lines mark the times of the FD onset. As an example, Figure 11 displays not only the FDs with MagnM 3.4 and 6.0 observed on December 1 and 31, 2014 that are marked by the green and yellow vertical lines but also two events with MagnM 2.1 and 2.7. Dashed and dotted horizontal lines give the pre-event values and the corresponding $3 \cdot \sigma$ uncertainty. From comparing both classes - the first one with $2 < \text{MagnM} \leq 3.0$ and the second one with MagnM >3.0 we find profound differences. For all four events, the count rate is decreasing. Taking into account the pre-event uncertainties, we find that the decreases are only larger than the uncertainty for the second class of events. In order to estimate the effectiveness of FD detection by the three NMs, we introduce the following qualitative assignments:

: indicates a significant decrease. The count rate decreases by a value of more than three standard deviations σ.

: indicates a decrease that is not significant, that is, the count rate decrease $\frac{\Delta c}{c}$ is larger than 2σ but smaller than 3σ

0: indicates no decrease that satisfies the upper criteria

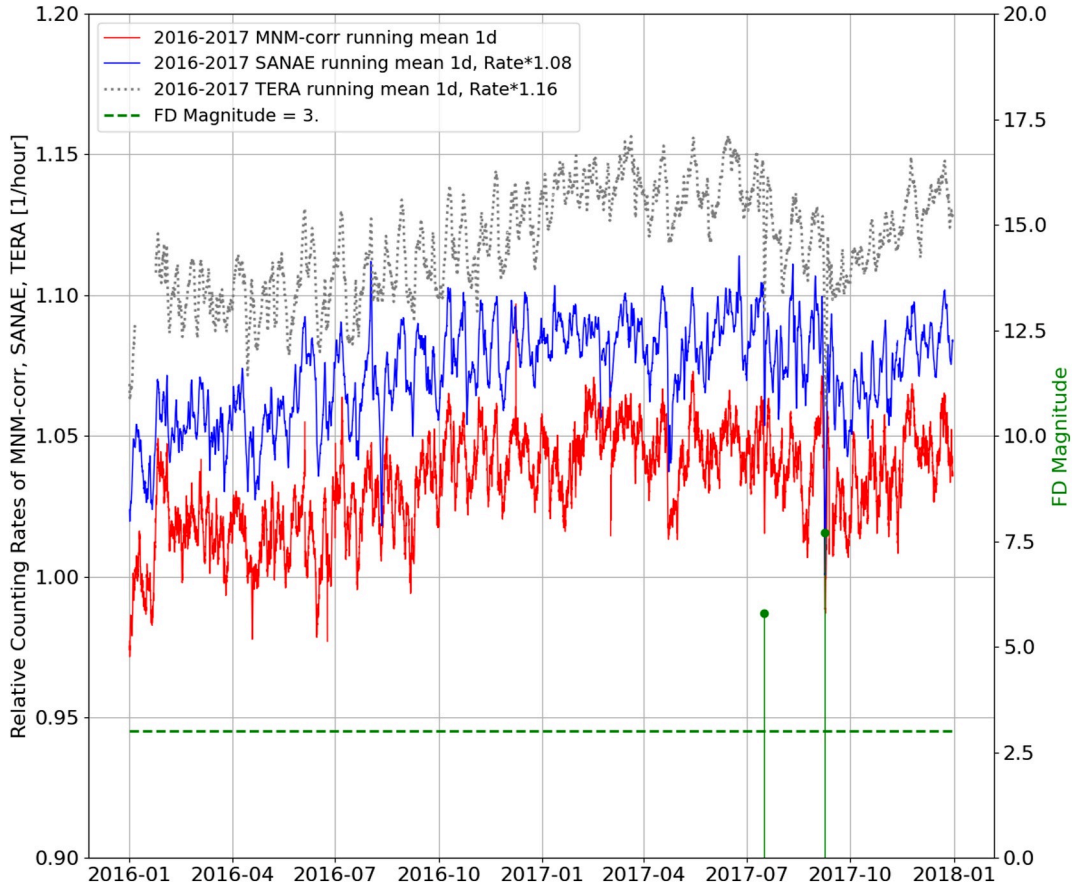

Figure 10. The daily averaged particle rates of the mini-neutron monitor, SANAE, and TERA Neutron Monitor for the years 2016 and 2017. The time positions of the Forbush Decreases with magnitudes MagnM >3 are indicated by green lines. The height of these vertical lines characterizes the magnitudes.

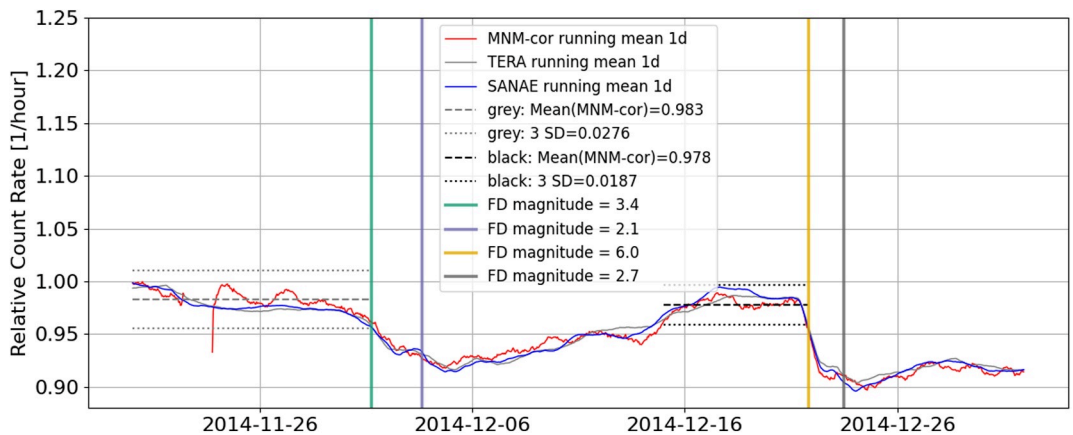

Figure 11. Daily running mean averaged count rates for the mini-neutron monitor (red curve), the SANAE (blue curve), and the TERA (gray curve) detectors based on hourly averages. Forbush Decreases (FDs) with MagnM 3.4 and 6.0 observed on December 1 and 31, 2014, respectively, are marked by the green and yellow vertical lines, respectively. The dashed and dotted lines give the pre-event values and the corresponding $3 \cdot \sigma$ uncertainty. In addition, two FDs from the IZMIRAN list are indicated by vertical lines with MagnM of 2.1 and 2.7, respectively (for details see text).

Table 5
Forbush Decreases (FDs) With a Magnitude MagnM > 3 Taken From the IZMIRAN Database

Date of FD	MagnM	Qual.Comp.	Fig.
2014.06.07 16:52	3.9	/ /	B1
2014.06.17 17:00	3.3	/ /	B1
2014.09.12 15:53	5.9	/ /	B2
2014.11.10 02:20	3.6	/ /	B3
2014.12.01 05:00	3.4	/ /	11
2014.12.21 19:11	6.0	/ /	11
2015.03.17 04:45	5.6	/ /	B4
2015.06.22 18:33	9.1	/ /	B5
2015.08.25 23:00	3.5	/ /	B6
2015.11.06 18:18	3.1	/ /	B7
2015.12.19 16:16	3.1	0/0/0	B8
2015.12.31 00:50	5.2	/ /	B8
2017.07.16 05:59	5.8	/ /	B9
2017.09.07 23:00	7.7	/ /	B10

Note. From left to right are provided the Date of the FD - Date and time of the FD onset, the MagnM - FD magnitude for particles with 10 GV rigidity, calculated as maximal range CR density variations in the event, the quality of detection for the mini-neutron monitor (M), SANAE (S) and TERA (T). Here means: significant, : indication, and 0: not seen. The last column gives the figure in which the event is shown.

In our example, we find that both count rate decreases with MagnM >3 are significant and therefore belong to the class . While the two other decreases belong to class for the SANAE and TERA NMs, they are class 0 for the MNM. The procedure has been repeated for all 14 FDs summarized in Table 5, giving the date and time of the FD onset, its MagnM from the IZMIRAN database (http://spaceweather.izmiran.ru/eng/dbs.html), a quality flag for the MNM, SANAE and TERA and the figure number, respectively. The quality flag is computed for each event from the mean values and the three standard deviation values of the MNM-cor count rate time profile before the FD onset. Each figure in Appendix B shows the full history of the event in question and gives an impression of the shape of the FD, its count rate drop, and recovery.

From our analysis, we find that from the 14 events investigated here 8, 5, and 1 are identified as , , and 0, respectively. From our analysis, we find that from the 14 events investigated here 8, 5, and 1 are identified as , , and 0, respectively. Thus, out of 14 events, 13 events were identified, and only one showed no decrease in these three NMs. Thus, we conclude tentatively that a MNM is well suited to support the analysis of FDs with amplitudes above 3%.

5. Summary and Conclusions

We evaluated the data from the MNM at the Neumayer III Antarctic research station from March 2014 to the end of 2017. The count rates were corrected for pressure variations using a coefficient β 0.00708/hPa. The pressure-corrected MNM measurements were compared to the TERA and SANAE NMs installed in Antarctica too. Especially in 2016, large differences between the MNM and the other two NMs were found. Thus, corrections for temperature and for variation of the HV were performed too. Since the results of these corrections were not conclusive and could not explain the above differences, we scaled the MNM 27-day running mean time profiles to a NM count rate time profile that has been computed from the weighted averages of the SANAE and TERA measurements. The choice of 27-day running mean averages assured that the long-term count rate profile is in agreement with the other NMs but does not affect the variations on the basis of a day. This was shown by the ratios of the normalized daily running mean counts of the three NMs. Here we find no systematic variation with time and computed for all three ratios, $\frac{c_{MNM}}{c_{SANAE}}$, $\frac{c_{MNM}}{c_{TERA}}$, and $\frac{c_{TERA}}{c_{SANAE}}$ a standard deviation of about 1%.

In order to investigate the sensitivity of the MNM at sea level, we investigated short-term decreases. Since the count rate of the MNM at sea level is more than 100 times smaller than the rates of TERA and SANAE, the statistical uncertainty has a standard deviation value of about 2.2%. This was improved by using a 1-day running mean count rate to an uncertainty of about 0.6%, allowing a comparison to the SANAE and TERA NMs.

The IZMIRAN database (http://spaceweather.izmiran.ru) of FDs was utilized for our study. 14 FDs with magnitudes MagnM >3 have been chosen for the observation period from March 2014 until the end of 2017. Computing the mean and the three standard deviation values of the MNM count rate distribution before the onset of an FD, a quality signature was defined. We found that for the three NMs from 14 FDs 13 FDs were identified: 8 of the 14 FDs were identified significantly, five were in the range of about 1 SD ("indication"), and only 1 was not seen.

These results allow us to draw the following conclusions:

- The pressure dependence of the count rates is in good agreement with the ones reported in the literature.
- The temperature dependence of the electronics and its influence on the count rate has almost no influence on the count rate distribution.
- An influence on the count rate variation of the order of days to 1 week is negligible, allowing an investigation of short-term flux variations.

- The GLE of 10 September 2017 showed an flux increase of 5% at TERA for a few hours. Given the statistical uncertainties of the MNM it is not possible to detect that event at sea level. However, a MNM was installed at 3,000 km height in Antarctica that registered the event because of its 18 times higher count rate.
- It could be shown that even at sea level, the MNM can identify FDs with MagnM >3 using the daily running mean count rates.
- The new electronics available since 2019 will improve the stability of data recording. Nevertheless, the ambient temperature should be stable within a few degrees to avoid day-night and long-term effects on the count rate.
- With its small size, low weight, and low power consumption, the MNM is an ideal detector for installation in rough terrain and makes it a cheap and effective alternative to large and heavy NMs (Krüger et al., 2015).

It should be mentioned that the data are provided by two web-based analysis tools: The NM database event search tool NEST (https://www.nmdb.eu/nest). There, the MNM data set can be selected under the name NEU3. Another analysis tool is the DESY outreach project Cosmic@Web (cosmicatweb.desy.de/ctplot/index_en.html). It was developed for school and university students to analyze data from many different cosmic particle detectors, including the MNMs on the Neumayer III research station and the German research vessel Polarstern.

Appendix A: Correction of Temperature Dependence and High Voltage

The mini-neutron monitor on Neumayer III was installed in a room where the temperature varies with the outside temperature. The maximum room temperature was about 28°C in Antarctic summer and about 12°C in winter.

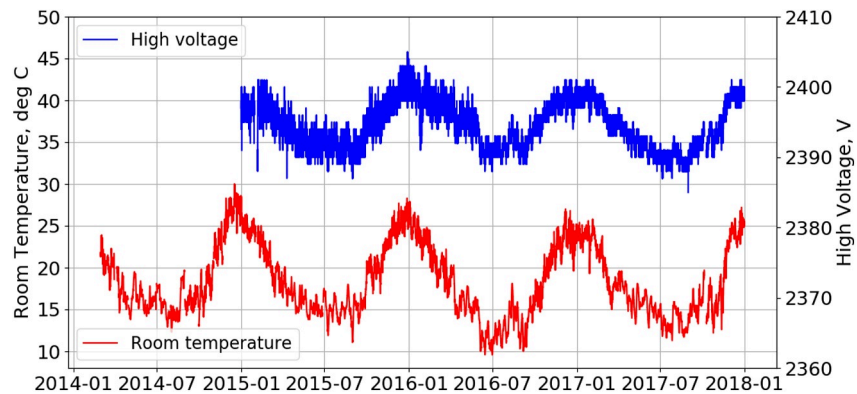

Figure A1. Room temperature (red) for the years 2014–2017 and high voltage (blue) for 2015–2017.

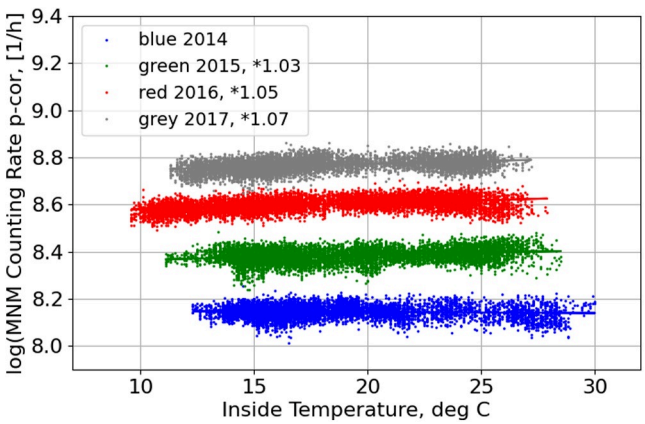

Figure A2. Dependence of the natural logarithm of the pressure-corrected mini-neutron monitor particle rates on the temperature for the years 2014–2017.

Figure A1 shows a clear seasonal correlation between the temperature and the high voltage (HV). Since the count rate for 2014 is comparable with that of 2015, the real HV setting of the tube was correct for 2014.

Since the air pressure and inside temperature are not correlated (not shown here) the temperature correction can be performed independently of the air pressure correction:

$Rate_{p,T\ corrected}$ $Rate_{pressure\ corrected} \cdot \exp(\ \beta \cdot (T$ $T_{mean})$. Figure A2 shows for every year the natural logarithm of the pressure-corrected particle rates in dependence on the temperature. The yearly temperature mean values and standard deviations are summarized in Table A1 together with the linear regression results. It is not understood, why the slope is for 2014 even negative and also for 2015 smaller than for the years 2016 and 2017. Therefore, it cannot be excluded that other unknown effects influenced the count rate of the MNM.

For the temperature correction, the fit results for 2014 were excluded, and only the mean values of T and slope β were chosen for the years 2015–2017.

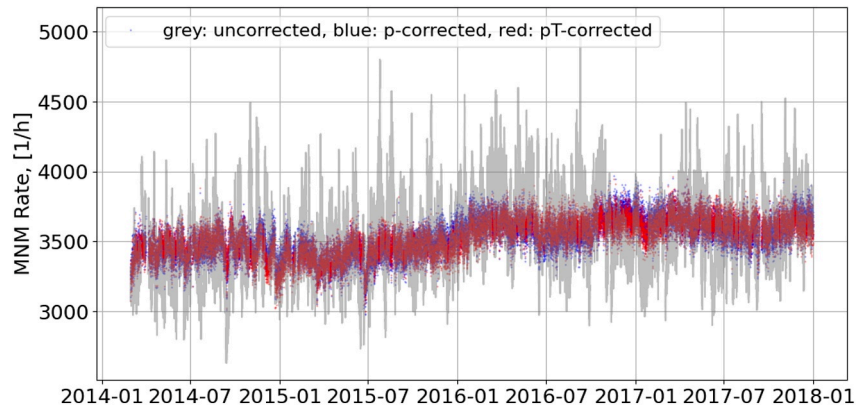

Figure A3. Uncorrected mini-neutron monitor (MNM) particle rate (gray), pressure-corrected count rate (blue), and (pressure- and temperature-corrected) MNM rate (red) for the years 2014–2017.

Table A1
Fit Values for the Different Years 2014–2017 and the Mean Values of 2,015–1,017

Fit results	2014	2015	2016	2017	Mean (2015–2017)
Mean Value T, °C	18.5	18.9	17.8	17.8	18.2
Standard Deviation	4.0	4.0	4.6	4.0	
Slope β, 1/(°C)	0.00047	0.00191	0.00237	0.00226	0.00218
Error	0.00008	0.00008	0.00006	0.00006	

Note. Rows 2 and 3: Mean Value and Standard Deviation of the Temperature Distributions. Rows 4 and 5: The Temperature Coefficient and Error of the Fits to the Yearly Distributions: log(MNM-Rate (Pressure-corrected) Vs. Temperature) Shown in Figure A2.

The results of the air pressure and temperature corrections are shown for the investigated period in Figure A3. The variation of the uncorrected count rate (gray) is reduced by the pressure correction, but the additional temperature correction has almost no influence on the shape of the count rate distribution. Therefore, an alternative correction method is presented in Section 3.

Appendix B: Forbush Decreases

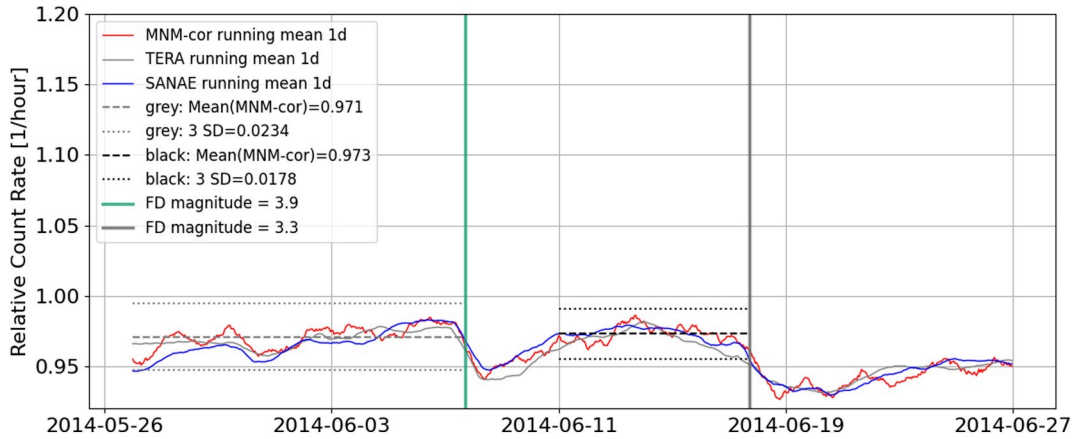

Figure B1. Daily running mean averaged count rates for the mini-neutron monitor (red curve), the SANAE (blue curve), and the TERA (gray curve) detectors based on hourly averages. Forbush Decreases with MagnM 3.9 and 3.3 observed on 7 June and 17 June 2014, respectively are marked by vertical lines. The dashed and dotted lines give the pre-event values and the corresponding 3σ uncertainty (for details see text).

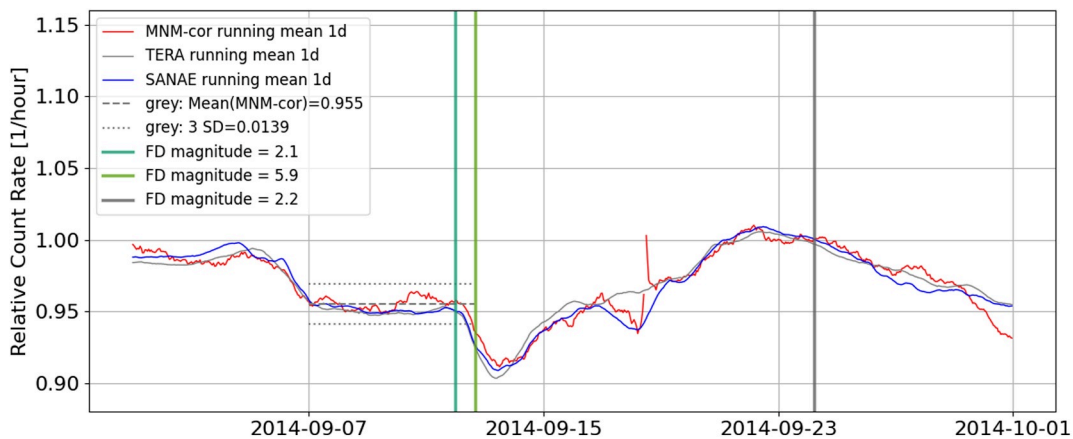

Figure B2. Same as in Figure B1 but for the Forbush Decrease (FD) on 12 September 2014 with a MagnM of 5.9 (light green line). During the period two FDs with a magnitude of MagnM of 2.1 (dark green line) and 2.3 (gray line) are listed by the IZMIRAN group. While the first one occurred just before the event the second one is separated by a few days. For both no significant decrease was obtained from the three Neutron Monitors.

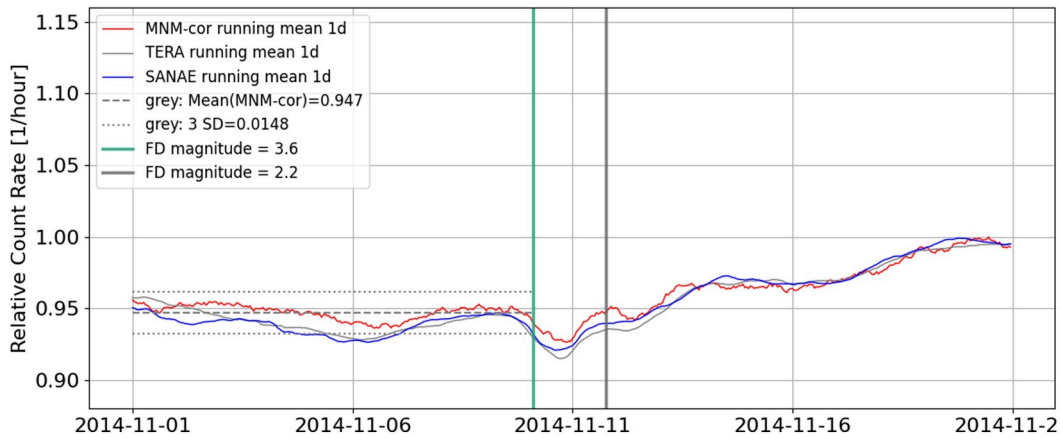

Figure B3. Same as in Figure B1 but for the Forbush Decrease (FD) on 10 November 2014 with a MagnM of 3.6 (dark green line). Another FD with a MagnM of 2.2 was reported a few days later. The event, however, did not produce a significant FD.

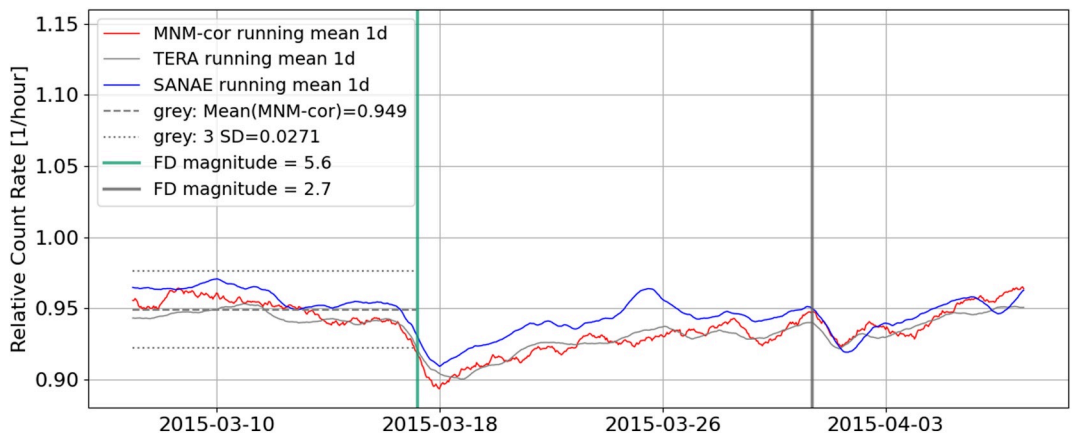

Figure B4. Same as in Figure B1 but for the Forbush Decrease (FD) on 17 March 2015 with a MagnM of 5.6 (dark green line). About 2 weeks later a FD with a MagnM of 2.7 (gray line) was measured by all three Neutron Monitors.

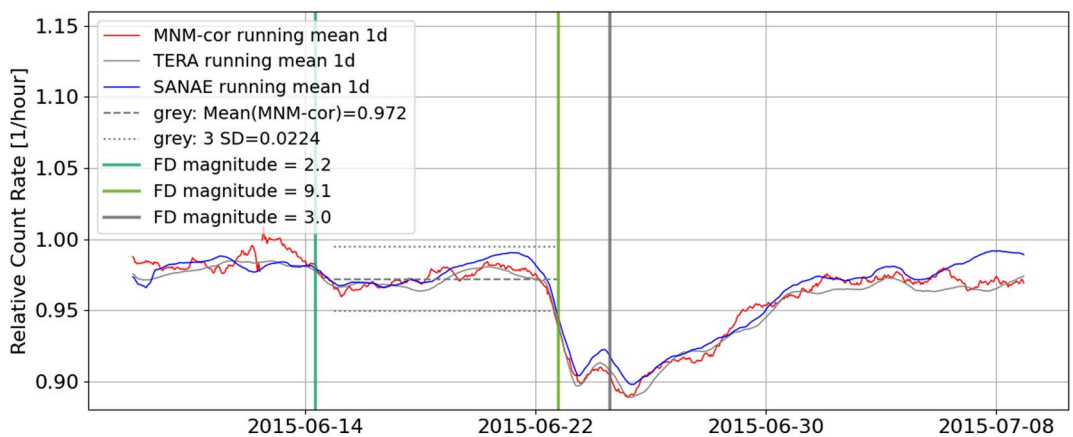

Figure B5. Same as in Figure B1 but for the Forbush Decrease (FD) on 22 June 2015 with a MagnM of 5.6 (light green line). Another two FDs with MagnMs of 2.2 (dark green line) and 3.0 (gray line) were registered by all three monitors too.

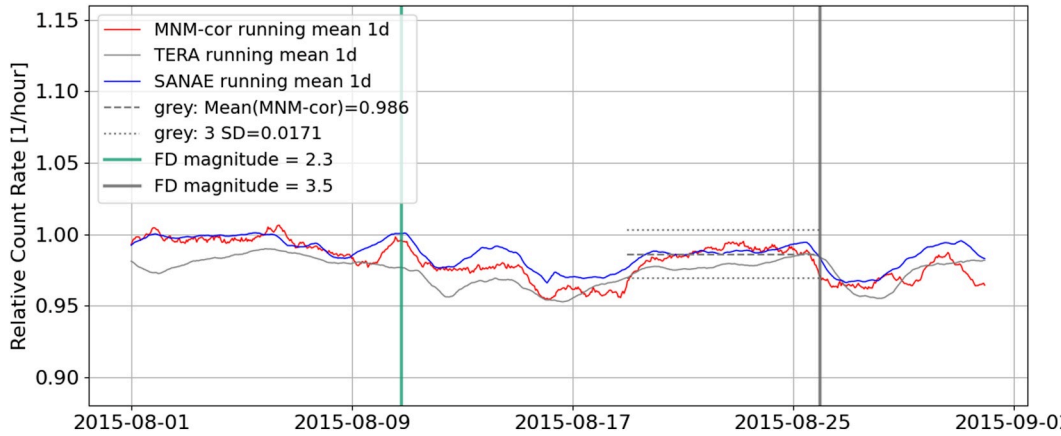

Figure B6. Same as in Figure B1 but for the Forbush Decrease (FD) on 25 August 2015 with a MagnM of 3.5 (gray line). The green line marks the time of a preceeding FD with an MagnM of 2.2. Both SANAE and the mini-neutron monitor indicate some flux decrease.

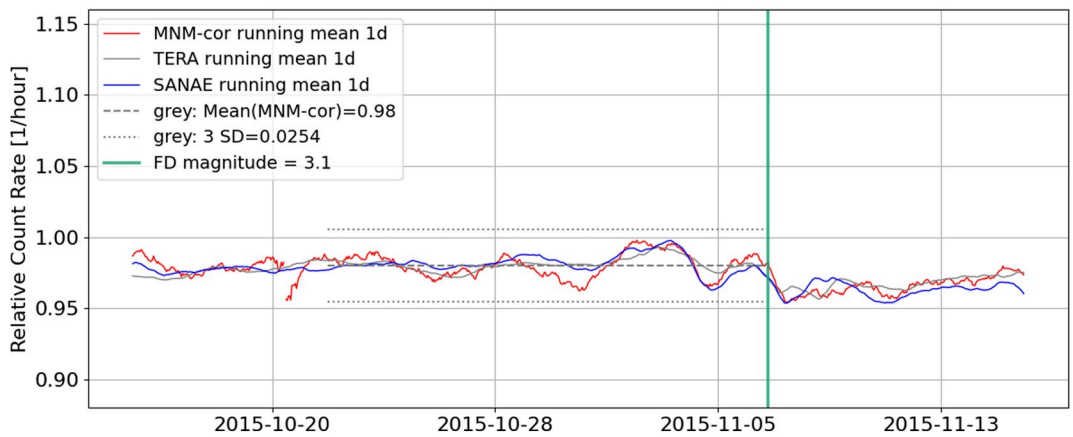

Figure B7. Same as in Figure B1 but for the Forbush Decrease on 6 November 2015 with a MagnM of 3.1 (green line).

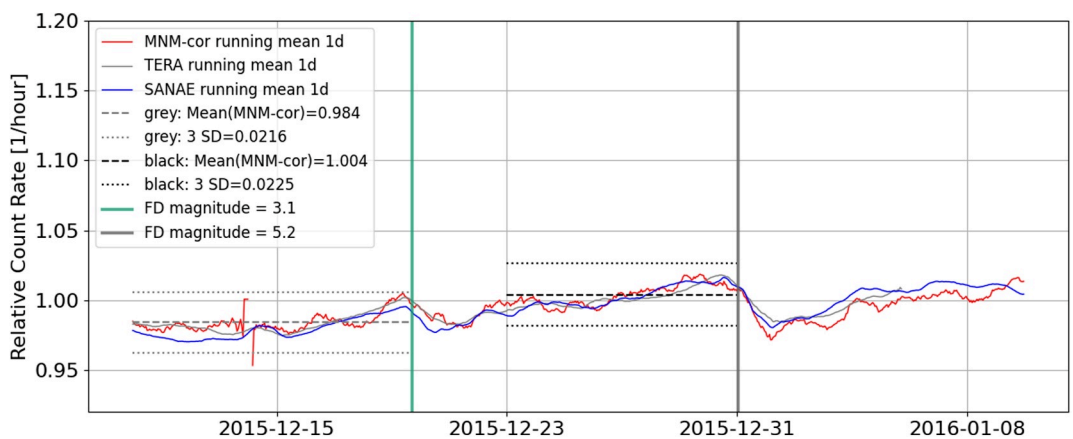

Figure B8. Same as in Figure B1 but for the Forbush Decrease on December 19 and 31 December 2015 with MagnMs of 3.1 (light green line) and 5.2 (gray line), respectively.

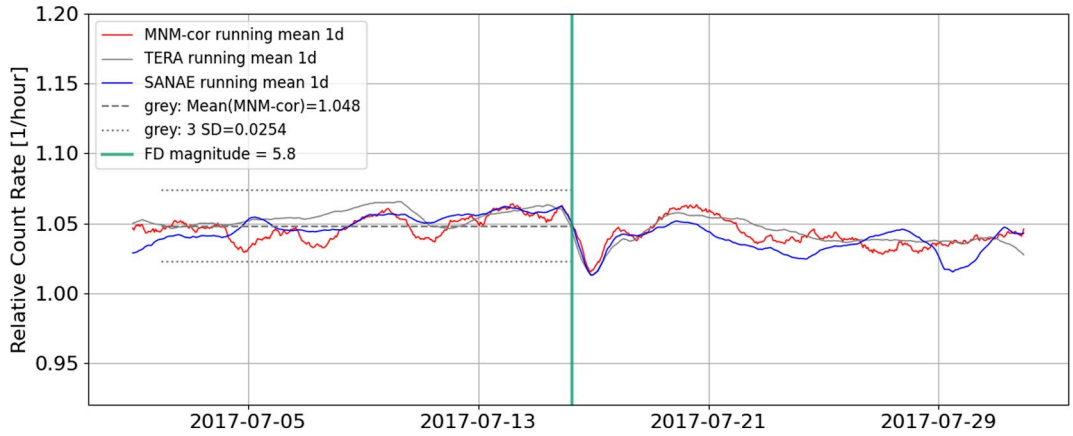

Figure B9. Same as in Figure B1 but for the Forbush Decrease on 16 July 2017 with MagnM of 5.8 (green line).

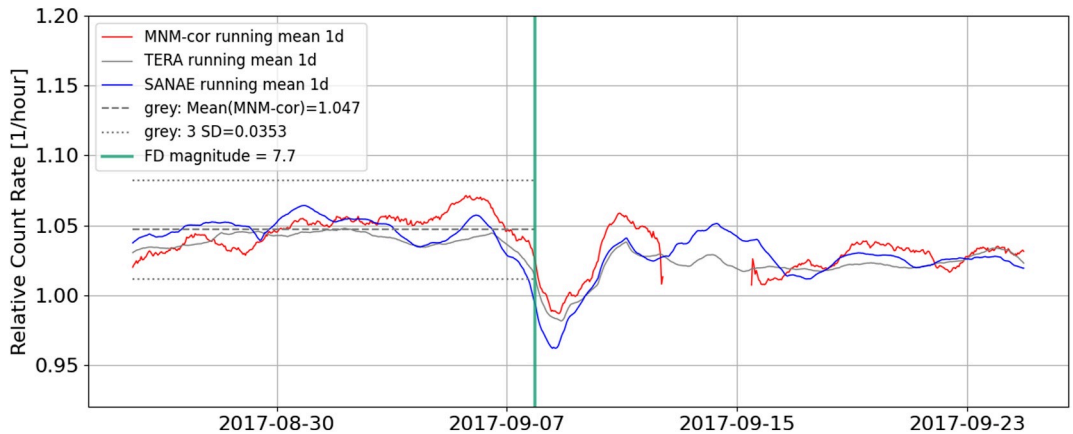

Figure B10. Same as in Figure B1 but for the Forbush Decrease on 7 September 2017 with MagnM of 7.7 (green line).

Acknowledgments
The installation and operation of the MNM on the German research station Neumayer III in Antarctica would not have been possible without the strong support of our colleagues from the AWI (Alfred-Wegener-Institut, Helmholtz-Zentrum für Polar-und Meeresforschung in Bremerhaven, Germany). We are very thankful for the possibility of using the data of the SANAE and TERA NMs provided by the NM Data Base (NMDB) (https://www.nmdb.eu/nest/), founded under the European Union's FP7 program (contract no. 213007). The authors acknowledge the IZMIRAN Space Weather Prediction Center, which provides the FD database. B.H. and K.H. further acknowledge the International Space Science Institute and the supported International Team 441: High EneRgy sOlar partICle EventsAnalysis (HEROIC) and the funding from the European Union's Horizon 2020 research and innovation program under grant agreement No 870405. Finally, we gratefully acknowledge the permanent support of our home institutions. Open Access funding enabled and organized by Projekt DEAL.

Data Availability Statement

Data Availability Statement The Neutron Monitor Data Base (NMDB) database gives access to Neutron Monitor data (www.nmdb.eu). The data are also available together with the weather data of the Neumayer III station via Cosmic@Web [6].

References

Belov, A. V. (2009). Forbush effects and their connection with solar, interplanetary and geomagnetic phenomena. In N. Gopalswamy & D. F. Webb (Eds.), *Universal heliophysical processes* (Vol. 257(S257), pp. 439–450). https://doi.org/10.1017/S1743921309029676

Bieber, J. W., Evenson, P., Dröge, W., Pyle, R., Ruffolo, D., Rujiwarodom, M., et al. (2004). Spaceship Earth observations of the Easter 2001 solar particle event. *The Astrophysical Journal Letters*, *601*(1), L103–L106. https://doi.org/10.1086/381801

Blanco, J. J., Hidalgo, M. A., Gómez-Herrero, R., Rodríguez-Pacheco, J., Heber, B., Wimmer-Schweingruber, R. F., & Martín, C. (2013). Energetic-particle-flux decreases related to magnetic cloud passages as observed by the Helios 1 and 2 spacecraft. *Astronomy & Astrophysics*, *556*, A146. https://doi.org/10.1051/0004-6361/201321739

Cane, H. V. (2000). Coronal mass ejections and Forbush decreases. *Space Science Reviews*, *93*(1), 55–77. https://doi.org/10.1007/978-94-017-1187-6_4

Desorgher, L., Kudela, K., Flückiger, E., Bütikofer, R., Storini, M., & Kalegaev, V. (2009). Comparison of Earth's magnetospheric magnetic field models in the context of cosmic ray physics. *Acta Geophysica*, *57*(1), 75–87. https://doi.org/10.2478/s11600-008-0065-3

Dumbović, M., Vrsnak, B., Calogović, J., & Zupan, R. (2012). Cosmic ray modulation by different types of solar wind disturbances. *Astronomy & Astrophysics*, *538*, A28. https://doi.org/10.1051/0004-6361/201117710

Eckner, A. (2015). Algorithms for unevenly spaced time series: Moving averages and other rolling operators. Retrieved from https://api.semanticscholar.org/CorpusID:18050741

Forbush, S. E. (1937). On the effects in cosmic-ray intensity observed during the recent magnetic storm. *Physical Review*, *51*(1), 1108–1109. https://doi.org/10.1103/physrev.51.1108.3

Heber, B., Galsdorf, D., Herbst, K., Gieseler, J., Labrenz, J., Schwerdt, C., et al. (2015). Mini neutron monitor measurements at the Neumayer III station and on the German research vessel Polarstern. *Journal of Physics: Conference Series*, *632*, 012057. https://doi.org/10.1088/1742-6596/632/1/012057

Hess, F., & Demmelmair, A. (1937). World-wide effect in cosmic ray intensity, as observed during a recent magnetic storm. *Nature*, *140*(3), 316–317. https://doi.org/10.1038/140316a0

Krüger, H., Moraal, H., & Benadé, G. J. J. (2013). Mini neutron monitors. In *International cosmic ray conference* (Vol. 33, p. 3666).

Krüger, H., Moraal, H., Bieber, J. W., Clem, J. M., Evenson, P. A., Pyle, K. R., et al. (2008). A calibration neutron monitor: Energy response and instrumental temperature sensitivity. *Journal of Geophysical Research*, *113*(A), 8101. https://doi.org/10.1029/2008ja013229

Krüger, H., Moraal, H., Nel, R., Krüger, H. G., & O'Kennedy, M. (2015). The mini neutron monitor programme. In *34th international cosmic ray conference (ICRC2015)* (Vol. 34, p. 223). https://doi.org/10.22323/1.236.0223

Krüger, P. P., Krüger, H. G., Krüger, H., Diedericks, C., & Malan, D. (2017). New, affordable, open-hardware neutron monitor electronics. In *35th international cosmic ray conference (ICRC2017)* (Vol. 301, p. 54). https://doi.org/10.22323/1.301.0054

Larsen, N., Mishev, A., & Usoskin, I. (2023). A new open-source geomagnetosphere propagation tool (OTSO) and its applications. *Journal of Geophysical Research: Space Physics*, *128*(3), e2022JA031061. https://doi.org/10.1029/2022JA031061

Lingri, D., Mavromichalaki, H., Belov, A., Eroshenko, E., Yanke, V., Abunin, A., & Abunina, M. (2016). Solar activity parameters and associated Forbush decreases during the minimum between cycles 23 and 24 and the ascending phase of cycle 24. *Solar Physics*, *291*(3), 1025–1041. https://doi.org/10.1007/s11207-016-0863-8

Matthiä, D., Heber, B., Reitz, G., Meier, M., Sihver, L., Berger, T., & Herbst, K. (2009). Temporal and spatial evolution of the solar energetic particle event on 20 January 2005 and resulting radiation doses in aviation. *Journal of Geophysical Research*, *114*(A), 8104. https://doi.org/10.1029/2009ja014125

Melkumyan, A., Belov, A., Abunina, M., Abunin, A., Eroshenko, E., Oleneva, V., et al. (2019). Recurrent and sporadic Forbush decreases during solar cycles 23–24. *Solar-Terrestrial Physics*, *5*(1), 28–34. https://doi.org/10.12737/stp-51201904

Mishev, A., Usoskin, I., Raukunen, O., Paassilta, M., Valtonen, E., Kocharov, L., & Vainio, R. (2018). First analysis of ground-level enhancement (GLE) 72 on 10 September 2017: Spectral and anisotropy characteristics. *Solar Physics*, *293*(10), 136. https://doi.org/10.1007/s11207-018-1354-x

Moraal, H., Belov, A., & Clem, J. M. (2000). Design and co-ordination of multi-station international neutron monitor networks. *Space Science Reviews*, *93*(1), 285–303. https://doi.org/10.1007/978-94-017-1187-6_14

Moraal, H., Krüger, H., Benadie, A., & de Villers, D. (2003). Calibration of the Sanae and Hermanus neutron monitors. In *Proceedings of the 28th international cosmic ray conference* (p. 3453).

Poluianov, S. V., Usoskin, I. G., Mishev, A. L., Shea, M. A., & Smart, D. F. (2017). GLE and sub-GLE redefinition in the light of high-altitude polar neutron monitors. *Solar Physics*, *292*(11), 176. https://doi.org/10.1007/s11207-017-1202-4

Richardson, I. G., & Cane, H. V. (2011). Galactic cosmic ray intensity response to interplanetary coronal mass ejections/magnetic clouds in 1995–2009. *Solar Physics*, *270*(2), 609–627. https://doi.org/10.1007/s11207-011-9774-x

Shea, M. A., & Smart, D. F. (2000). Fifty years of cosmic radiation data. *Space Science Reviews*, *93*(1), 229–262. https://doi.org/10.1007/978-94-017-1187-6_12

Simpson, A. (2000). The cosmic ray nucleonic component: The invention and scientific uses of the neutron monitor–(Keynote Lecture). *Space Science Reviews*, *93*(1), 11–32. https://doi.org/10.1023/a:1026567706183

Strauss, D. T., Poluianov, S., van der Merwe, C., Krüger, H. G., Diedericks, C., Krüger, H., et al. (2020). The mini-neutron monitor: A new approach in neutron monitor design. *Journal Space Weather Space Climate*, *10*(39), 12. https://doi.org/10.1051/swsc/2020038

Tsyganenko, N. A. (1989). A magnetospheric magnetic field model with a warped tail current sheet. *Planetary and Space Science*, *37*(1), 5–20. https://doi.org/10.1016/0032-0633(89)90066-4

Usoskin, I. G., Bazilevskaya, G. A., & Kovaltsov, G. A. (2011). Solar modulation parameter for cosmic rays since 1936 reconstructed from ground-based neutron monitors and ionization chambers. *Journal of Geophysical Research*, *116*(A), 2104. https://doi.org/10.1029/2010ja016105

Wang, S., Bindi, V., Consolandi, C., Corti, C., Light, C., Nikonov, N., & Kuhlman, A. (2023). Properties of Forbush decreases with AMS-02 daily proton flux data. *The Astrophysical Journal*, *950*(1), 23. https://doi.org/10.3847/1538-4357/acca1b